

Metallurgical Analysis of Cracked AA7075 Aluminum Alloy Component Used in Control System of a Satellite Launch Vehicle

Sushant K. Manwatkar · J. Srinath · S. V. S. Narayana Murty ·
P. Ramesh Narayanan · S. C. Sharma · P. V. Venkitakrishnan

Submitted: 23 July 2016/in revised form: 4 October 2016/Published online: 9 November 2016
© ASM International 2016

Abstract High-strength aluminum alloy AA7075 forgings are widely used in various control system components of liquid engines of satellite launch vehicles. In one such application, a forged component was found to crack under storage. Multiple cracks were noticed on the surface of the component. Fractographic features indicated intergranular mode of failure. Optical microscopic examination revealed dendritic coring in the material and crack propagation to be along the grain boundaries. Anodic dissolution of grain boundaries was also noticed. Based on detailed metallurgical investigations, it was concluded that the failure was due to ‘stress corrosion cracking.’

Keywords AA7075 alloy · Intergranular cracking · Dendritic Coring · Stress corrosion cracking

Introduction

Aluminum alloy AA7075 (Al–5.5Zn–2.5 Mg–1.5Cu) is widely used in the fabrication of aerospace structural components in view of its high strength coupled with excellent corrosion resistance. This alloy is non-weldable and is strengthened by precipitation hardening. Different types of structural components for control systems of liquid

engines of satellite launch vehicles are fabricated out of this alloy. In one such critical application, a secondary injection thrust vector control valve body was found to be cracked during the routine visual inspection. The component was machined out of a cylindrical forged block and was anodized after fabrication. The component has cracked during storage. This paper brings out the details of metallurgical investigations carried out to establish the reason for cracking.

Experimental

The cracked surface was carefully separated by sectioning the component to analyze the topographical features of the fracture surface using a Carl Zeiss EVO-50 scanning electron microscope (SEM). The portion containing the crack was also sectioned for metallographic analysis. The metallographic specimens were mounted and polished using a series of SiC emery papers and final polishing was carried out with half-micron diamond lapping compound. The finish polished specimens were etched using Keller’s reagent (2 ml HF, 3 ml HCl, 5 ml HNO₃, 190 ml H₂O) to reveal the microstructural features. The metallographic specimens were observed using Olympus GX-71 inverted optical metallurgical microscope. An Oxford-INCA Energy dispersive X-ray spectrometer was used to obtain the chemical composition on the fracture surface. Electron probe micro-analyzer (EPMA) JEOL JXA-8530F was used to analyze the elemental segregation in the material. Transmission electron microscopy (TEM) analysis of precipitates was carried in 200 kV JEOL equipment. The microstructure was also observed under a Bruker atomic force microscope (AFM) in contact mode. Nanoindentation

S. K. Manwatkar · J. Srinath · S. V. S. N. Murty (✉) ·
P. R. Narayanan · S. C. Sharma · P. V. Venkitakrishnan
Materials and Mechanical Entity, Vikram Sarabhai Space
Centre, Trivandrum 695 022, India
e-mail: susarla.murty@gmail.com

studies were carried out to understand the variation in hardness in the cored regions and normal regions in the microstructure using a CSM Instruments nanoindentation testing machine. All indentations were performed using a Berkovich diamond indenter using a standard cycle with loading and unloading time of 30 s each with a hold time of 10 s at maximum load. A matrix of 64 equally spaced indentations was made with a maximum load of 10 mN. Hardness was evaluated using Oliver and Pharr method.

Observations and Discussion

Observations

The visual observations on the cracked component indicated four cracks on the top face of the component. The cracks were in radial direction with respect to the original cylindrical forging. All the four cracks have started from the outer periphery of the component and propagated in both longitudinal and radial directions. The digital photograph of the cracked component is shown in Fig. 1, and the cracks are highlighted and marked as 1, 2, 3, and 4 on the component.

SEM observations on the crack location revealed the crack initiation to be from the outer periphery of the

component. At the outer periphery corner of the component, deep machining marks were observed and corrosion pits were noticed at the deep machining marks (Fig. 2). Severe damage to the anodized layer was also noticed (Fig. 3). Dissolution of few grains along the crack path is shown in Fig. 4, which led to the formation of cavities. The

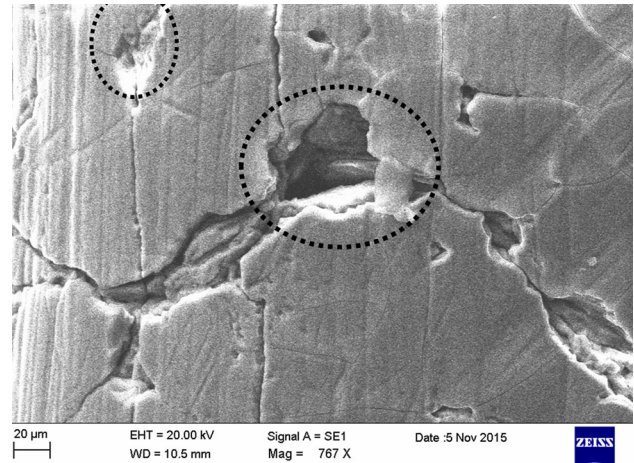
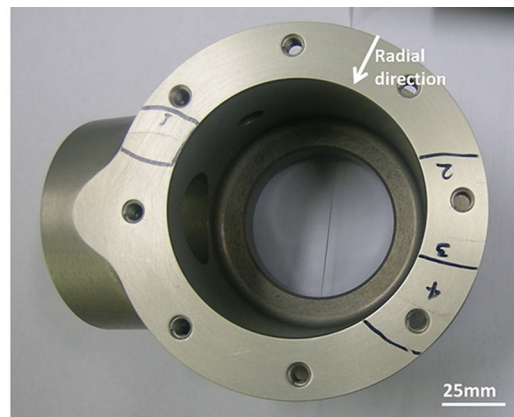
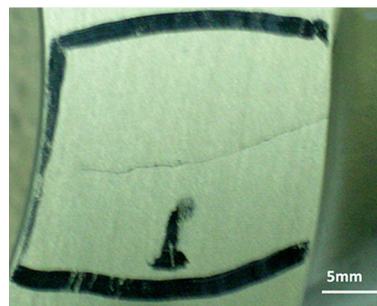


Fig. 2 Scanning electron micrograph showing corrosion pits at crack initiation site and deep machining marks on the surface. The corrosion pits are encircled with dotted circle. The vertical lines are machining marks

Fig. 1 Digital photograph of the cracked component showing 4 nos. of cracks. The cracks have started from outer periphery and propagated in with longitudinal and radial directions



(a)



(b)



(c)

SEM observation of the fracture surface revealed the presence of corrosion products throughout (Fig. 5). The presence of corrosion products on the fracture surface camouflaged the fractographic features underneath, and it was essential to remove them for conducting the failure analysis. In order to remove the corrosion products, the fracture surface was cleaned with nitric acid solution as per the guidelines provided in ASTM G1-03. The procedure for cleaning the fracture surface involves immersing the specimen in a 1:1 solution of HNO₃:H₂O for 10 minutes followed by washing the specimen with demineralized water. The cleaned surface was dried by blowing hot air on to the surface. The observations after the cleaning of

fracture surface revealed intergranular features with the cracks along the grain boundaries (Fig. 6).

The optical microscopy of the polished and etched specimens revealed the presence of coring (elemental micro segregation) in the material indicated as dark flowery patterns. The flowery patterns were more evident in the optical photomicrographs taken in the dark field mode (Fig. 7b). The grain boundaries were decorated with precipitates (Fig. 7a). The grain boundaries also had an extensive network of sub-grains as shown in optical photomicrographs taken in the dark field mode (Fig. 8). The optical microscopic observations of the cracks indicated intergranular nature of cracking with extensive crack

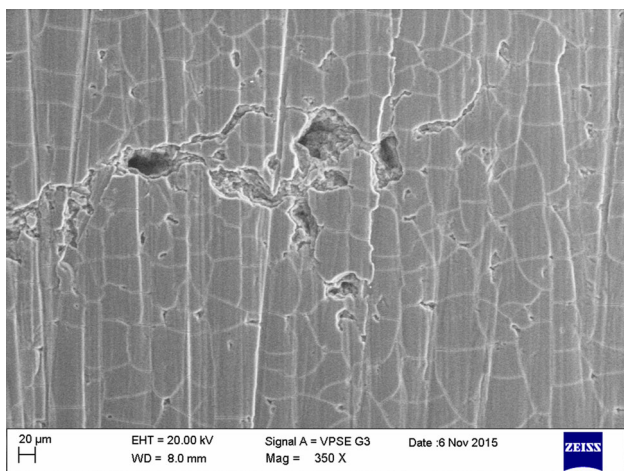


Fig. 3 Scanning electron micrograph showing the damage on the anodized layer. The general structure seen corresponds to the anodized layer which is damaged at certain locations

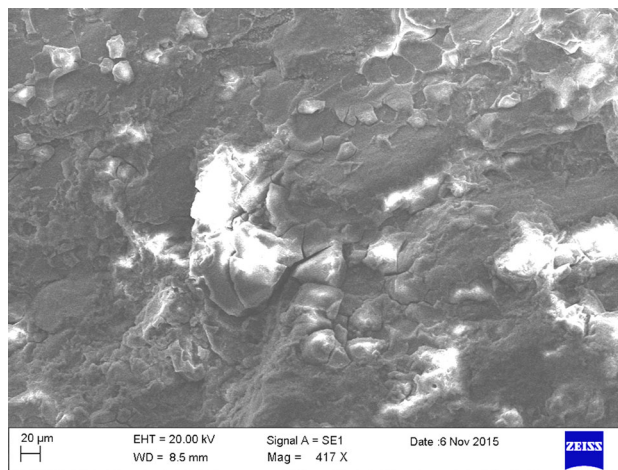
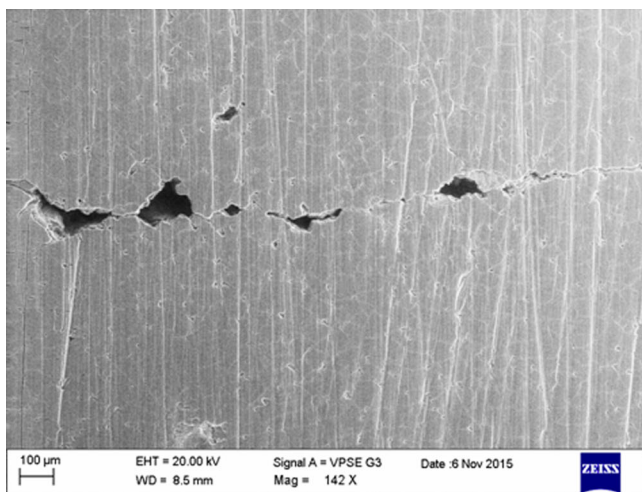
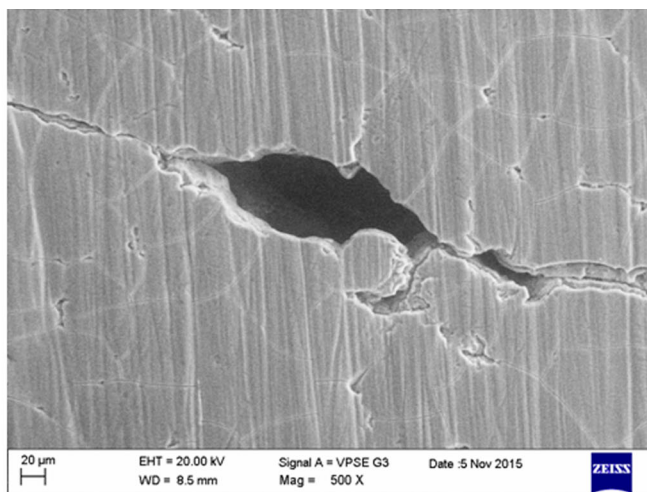


Fig. 5 Scanning electron micrograph showing the presence of corrosion products on the fracture surface. Since the corrosion products are electrically non-conducting in nature, charging takes place at the location where these products are present

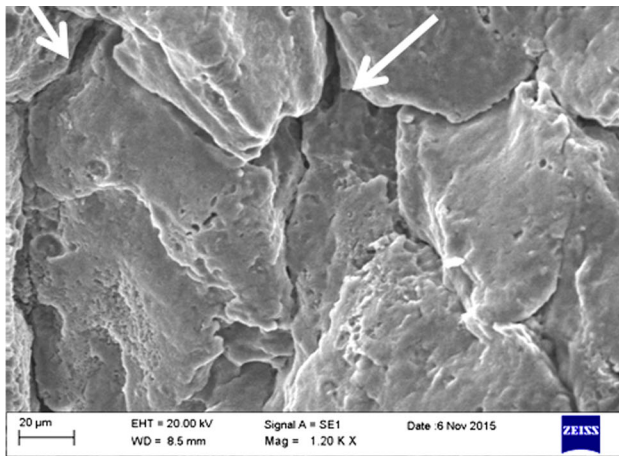


(a)

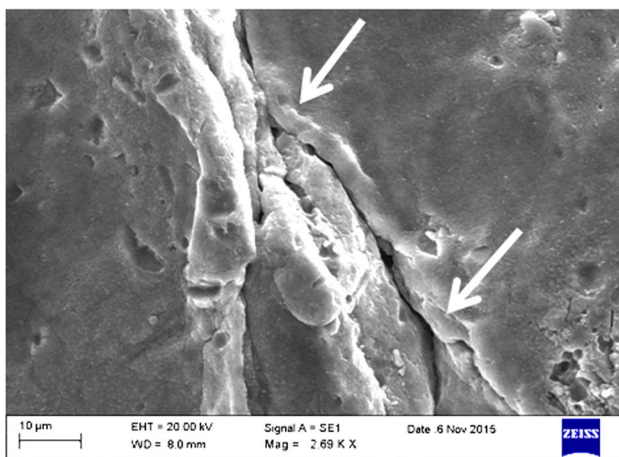


(b)

Fig. 4 Scanning electron micrographs showing dissolution of grains along the crack path, leading to the formation of cavities. The photographs are taken at two different magnifications (**a**, **b**)



(a)



(b)

Fig. 6 Scanning electron micrographs of the fracture surface showing the intergranular features (a) with the cracking along the grain boundaries (b)

branching (Fig. 9a). The anodic dissolution at grain boundaries was also noticed (Fig. 9b). Grain separations along the crack path were also noticed as shown in Fig. 9c. Higher magnification observation revealed precipitation along the grain boundaries (Fig. 9d).

In order to understand the role of dendritic coring on the failure of the component, it is essential to study the nature and extent of segregated elements. For this purpose, specimens prepared for optical microscopy were taken up for EPMA analysis. Elemental microanalysis was carried out on dark cored regions and light regions (devoid of any segregation) by point mode chemical analysis and line scan for compositional gradient. The observations on the dark cored regions indicated coarse precipitates (Fig. 10a). The light areas were devoid of these coarse precipitates (Fig. 10b). The elemental segregation in the cored region and light region was analyzed by obtaining the chemical composition of the selected areas marked by red circle in

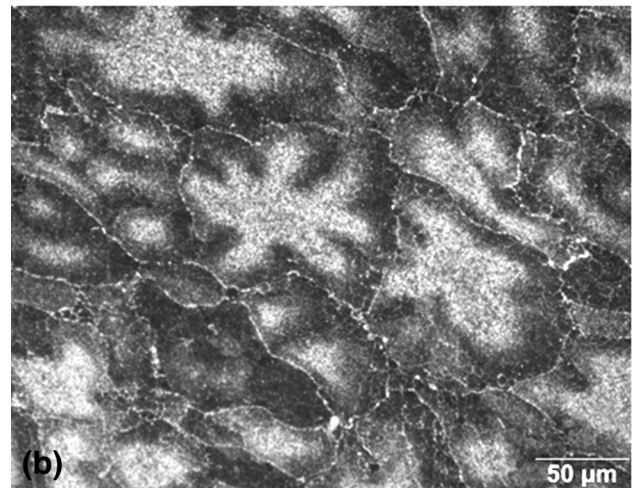
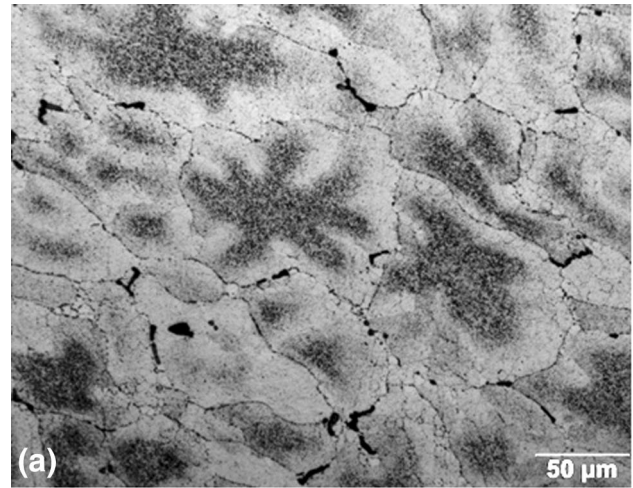


Fig. 7 Optical photomicrographs showing the (a) precipitates along the grain boundaries (b) flowery pattern and grain boundaries are more evident in dark field mode

Fig. 10. The chemical composition obtained by the EPMA analysis is given in Table 1. The results show the segregation of chromium in the cored region. Figure 11 shows the line scan from light region to cored region (as marked by green lines in Fig. 11a) and distribution of chromium across the line (Fig. 11b). The TEM observations indicate the precipitation of $MgZn_2$ along the grain boundaries and in the matrix (Fig. 12).

In order to understand the effect of dendritic coring on the local mechanical properties, measurement of hardness of the dark (cored) and light (uncored) regions was studied. Since the cored regions are at most 50 microns in size, microhardness is not suitable for measurement of hardness. Therefore, nano-indentation testing was adopted in the present study. The measurements were made from a matrix of equally spaced indentations as shown in the optical photomicrograph Fig. 13a. Figure 13b shows the indentations falling on dark cored regions and light regions. Figure 13c and d show high-magnification optical

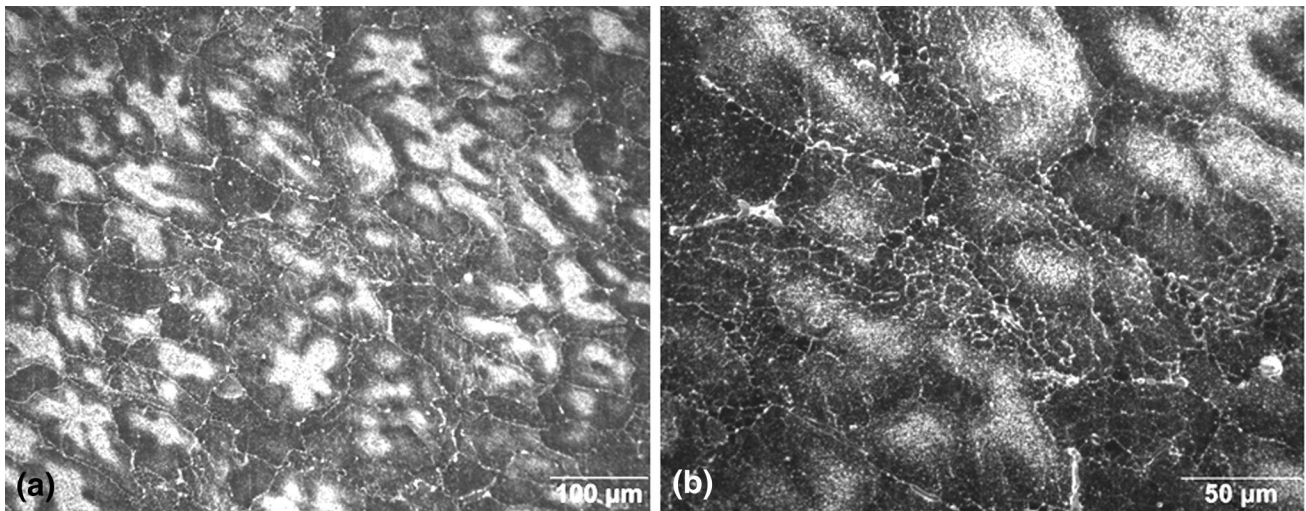


Fig. 8 Optical photomicrographs taken in dark field mode showing extensive network of subgrains along the grain boundaries. The photographs are taken at two different magnifications

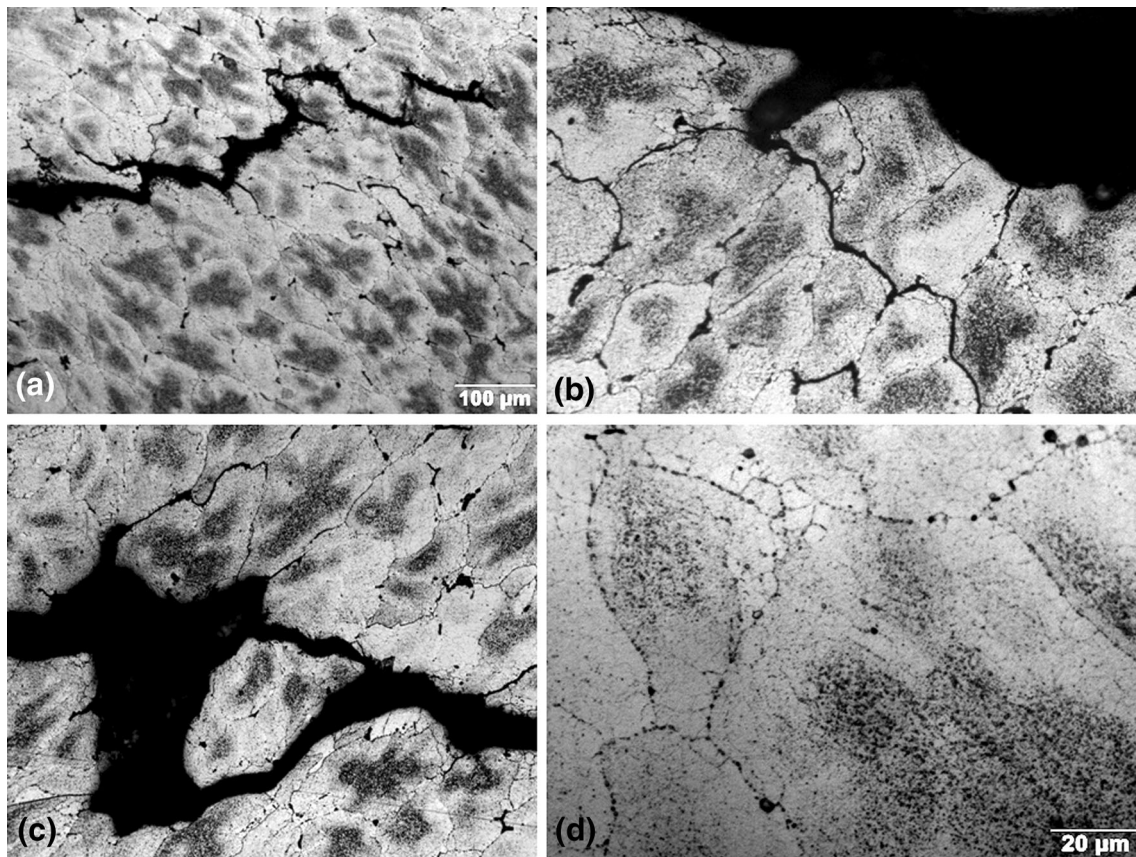


Fig. 9 Optical photomicrographs taken at the crack location showing (a) intergranular nature of cracking, (b) anodic dissolution at grain boundaries, (c) grain separations along the crack path and (d) precipitation along the grain boundaries

micrographs at dark cored region and light region. The nano indentation results indicated the average hardness of the dark cored area was 2190 MPa and for light areas, the

hardness was 2530 MPa. The load-depth curves at dark cored region and light region are shown in Fig. 14. Load-depth curves indicate that the depth of penetration in the

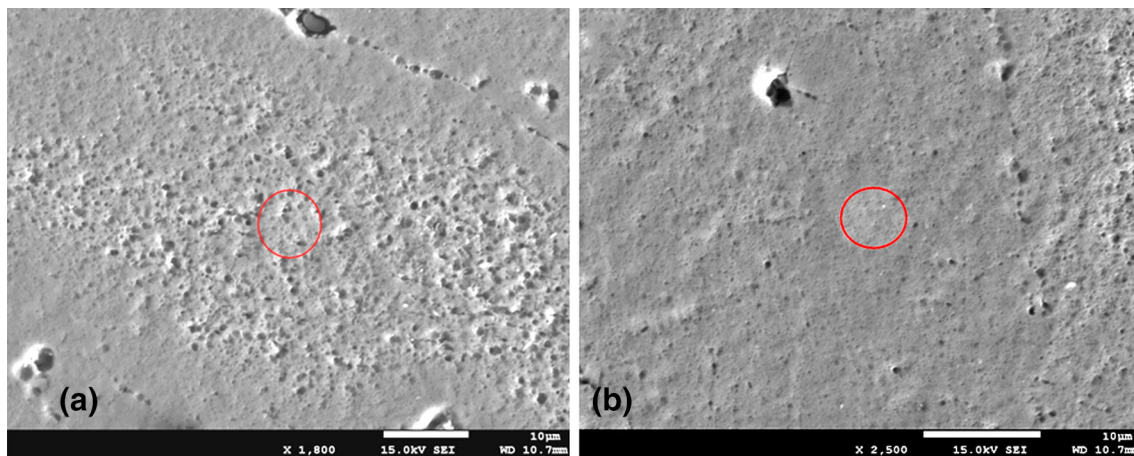


Fig. 10 Photomicrographs taken in electron probe micro analyser at (a) dark cored region showing coarse precipitation (b) light region devoid of coarse precipitation

Table 1 The chemical composition at cored region in wt.% obtained by EPMA

Elements	Zn	Mg	Cu	Cr	Mn	Si	Ti	Al
Dark cored region	5.870	2.557	1.653	0.357	0.016	0.016	0.008	Balance
Light region	5.633	2.557	1.683	0.144	0.011	0.013	0.007	Balance

dark cored region was higher than light regions in the microstructure. AFM image of the microstructure of the alloy is illustrated in Fig. 15. The image shows coarse precipitation (indicated by the localized blue dots in the cored regions) in cored microstructure.

Discussion

The forged component has cracked at four different places. The crack initiations were from the outer periphery corner of the component propagating in both longitudinal and radial directions. The SEM observations at the crack locations revealed the presence of corrosion pits near the outer periphery corner of the component. Deep machining marks were also noticed at this location. Higher speed and depth of cut can lead to deep machining marks. The anodized layer near to these deep machining marks may not be continuous and perfect and leads to easy initiation of corrosion pits. There was a time gap of about 9 months between the component forging and anodization during which the material was in unprotected condition under humid conditions. The humid and marine environment (Trivandrum, Kerala, India) of the storage location has helped in the formation of corrosion pits. Pitting attack in aluminum alloys occurs in water containing chlorides particularly at crevices or stagnant areas where the breakdown of passivity can be accelerated due to differential aeration effects [1]. In the present case, deep machining

marks acted as crevices and were further attacked by moisture and presence of chlorine in marine atmosphere. The environments that caused stress corrosion cracking (SCC) are generally aqueous and condensed layer of moisture usually forms on the surface due to the high humidity in marine environment [2].

The presence of corrosion products on the fracture surface indicated the role of corrosion in crack initiation and propagation. Detailed optical and SEM observations indicated that cracks were initiated from the corrosion pits and propagated inward in an intergranular mode with severe crack branching along the crack paths. The network of precipitates along the grain boundary was responsible for the preferential grain boundary dissolution (Fig. 9). Precipitation at the grain boundary was confirmed by optical and transmission electron microscopy. Grain separations were noticed along the crack path due to the complete dissolution of grain boundaries. The $MgZn_2$ precipitates present at the grain boundaries are more anodic to the matrix which results in a local cell action at the grain boundaries leading to selective dissolution of grain boundaries by electrochemical mechanism [3, 4]. The large network of sub-grains along the grain boundaries as shown in Fig. 8 has also provided additional sites for preferential precipitation at sub-grain boundaries. The $MgZn_2$ precipitation along the grain boundaries was responsible for the anodic dissolution of grain boundaries in the presence of residual stresses in the material.

The AA7075 alloy in T7 condition is considered to have improved short transverse stress corrosion cracking resistance [5–8]. This alloy in peak-aged (T6) condition is more

susceptible to SCC. The precipitates in the over aged condition are not continuous along the grain boundaries as compared to continuous grain boundary precipitates in T6 condition. In T6 condition, the precipitates are predominantly intermediate metastable precipitate (η) and change to equilibrium η ($MgZn_2$) coarse precipitates on further aging to T73 condition. However, the quenching rate and delay between the quenching and aging are very important factors during heat treatment operation. The resistance to corrosion and stress corrosion cracking improves by rapid rate of quenching with minimum quench delay. The precipitation during slow rate of quenching generally occurs on the high-angle grain boundaries. These grain boundary precipitates provide a preferential crack path during stress corrosion cracking. During aging process, GP zones may nucleate homogeneously and precipitates develop sequentially in the matrix, but the presence of grain boundaries, sub-grain boundaries, and dislocations alter the free energy leading to significant heterogeneous nucleation either during quenching or aging above GP zone solvus temperature. Above this temperature, semi-coherent transition precipitates nucleate and grow directly on the dislocations and sub-grain boundaries and incoherent equilibrium precipitates nucleate and grow on the high-angle grain boundaries [3].

The concentration of dispersoid-forming elements like chromium should be kept to the minimum required to control the grain structure to impart improved toughness. 7XXX alloy sheet was reported to have shown considerable reduction in toughness with increase in chromium concentration. Chromium has a slow diffusion rate and forms fine dispersoid phases which inhibit the nucleation/grain

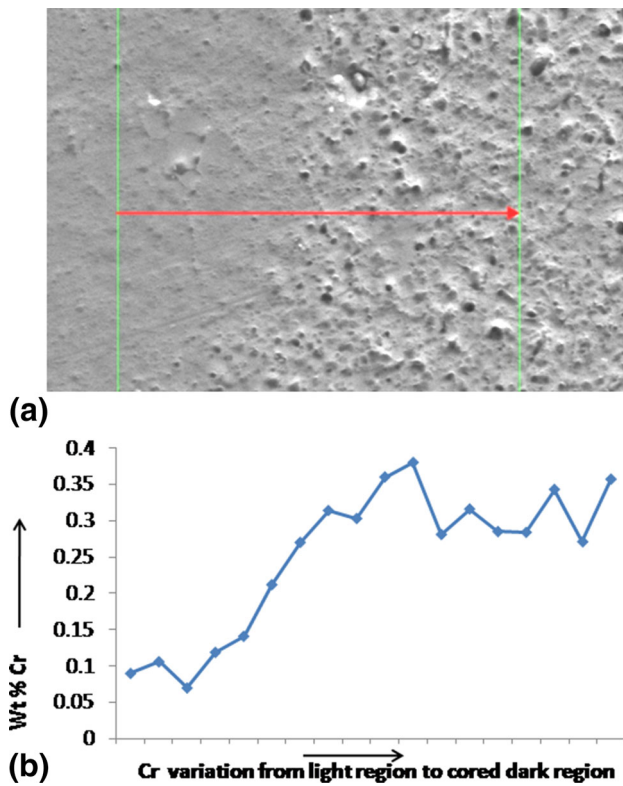


Fig. 11 Photomicrograph taken in EPMA showing (a) the area considered for obtaining line scan from light region (uncored) to dark region (cored) and (b) distribution of chromium from light region to dark cored region

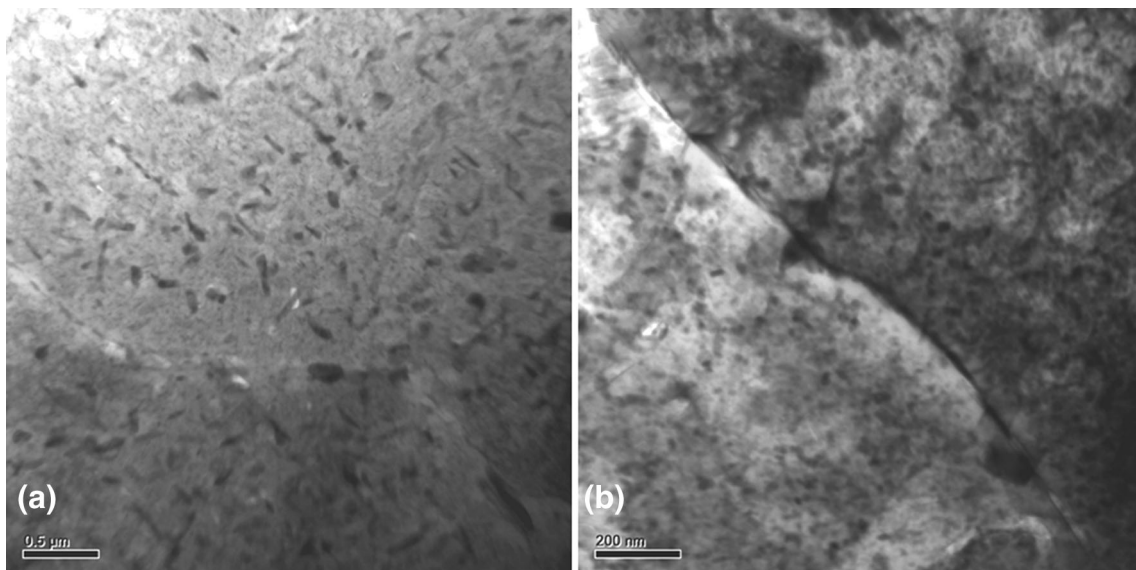


Fig. 12 Transmission electron micrographs showing the precipitation at the grain boundaries and in the matrix. The precipitates correspond to $MgZn_2$

growth and hence used to prevent the recrystallization in 7XXX alloys. Major drawback of chromium in this alloy is that it increases the quench sensitivity and hardening phase tends to precipitate on the pre-existing chromium-phase particles [3]. In the present study, the observation of flowery features and segregation of chromium in those regions are indicated by detailed EPMA analysis on the cored regions and light regions in the microstructure. Higher concentration of chromium was reported in cored regions of AA7075 alloy [9]. The segregation of chromium at cored regions could have been responsible for initiation of precipitation on the chromium phase particles during quenching itself, which have subsequently grown during aging. This resulted in the differential precipitation across the cored regions. This phenomenon led to very coarse precipitation at the cored regions as indicated by EPMA and AFM observations.

Nano-indentation results indicated that the hardness was lower in cored region than the lighter (uncored) region. This observation also suggests that the cored regions have very

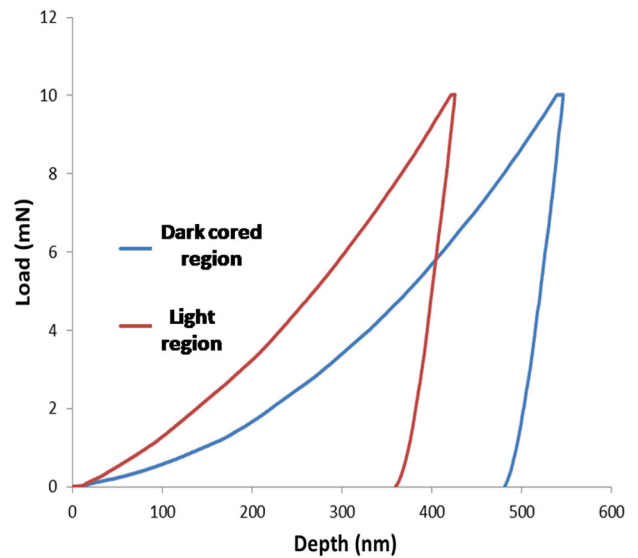


Fig. 14 Load-depth curves from dark cored region and light region obtained from nano-indentation test

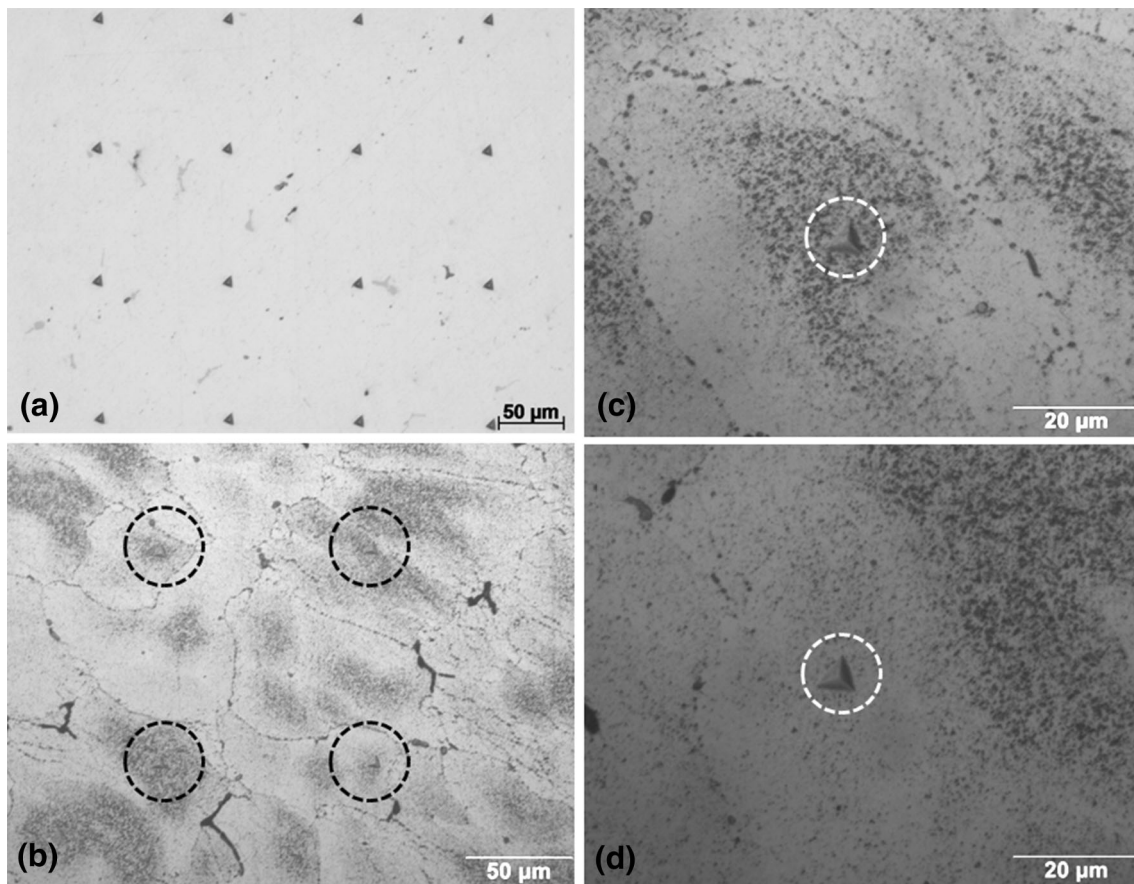


Fig. 13 The optical photomicrographs nano indentations (a) matrix of indentation, (b) indentations at dark cored region and light region, (c) high magnification view of indentation at dark cored region (d) high magnification view of indentation at light region. The indentations are marked by circles in the photographs

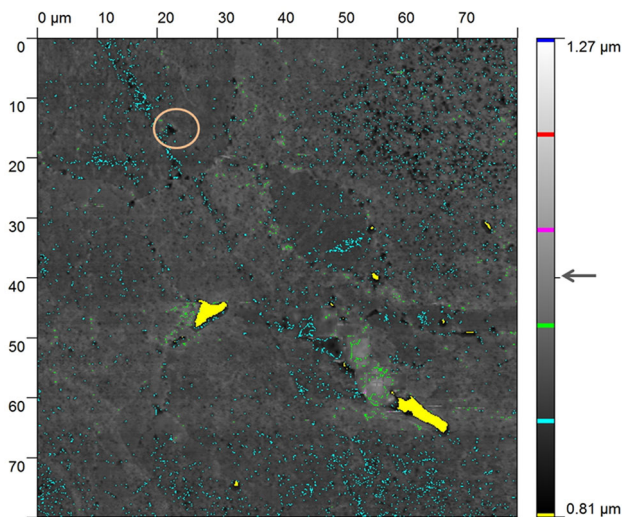


Fig. 15 AFM image of the microstructure showing the dark cored region with coarse precipitations, nano indentation is marked by a circle

coarse and non-coherent precipitates responsible for reduction in hardness at these regions. However, the presence of chromium segregation led to differential precipitation across the microstructure. This can result in the manifestation of regions of coherent precipitates representative of T6 condition and regions of semi-coherent/non-coherent precipitates representative of T7 condition. These two types of regions co-exist together and led to reduction in resistance to stress corrosion cracking. The cored regions are also responsible for easy formation of corrosion pits during the initial stages of stress corrosion cracking.

The anodic dissolution of grain boundaries occurs due to the electrochemical mechanism under the presence of stresses. The stresses can be applied stresses like assembly stresses, service stresses, or it can be residual stresses. In the present study, no applied or assembly stresses were present because the component has cracked in storage condition, but the presence of residual stresses in the material could not be ruled out. In this alloy, the residual stresses can be generated by quenching operation during solutionizing treatment. The residual stresses generated during quenching operation are relieved by 2–4% cold compression and the material is overaged to impart T7352 temper. If the cold compression is not carried out properly, the residual stresses can be still present in the material which can induce favorable condition for stress corrosion cracking. In the present case study, the corrosion pits were responsible for crack initiation and propagated under the influence of residual stresses. The micro segregation of alloying elements, extensive sub-grain structure, and precipitation along the grain boundary were favorable conditions for stress corrosion cracking.

Conclusions

Based on detailed metallurgical analysis, the cracking of AA7075 alloy-forged component was attributed to stress corrosion cracking. The following factors were responsible for stress corrosion cracking of the component:

1. Deep machining marks on the outer periphery of the component acted as crevices and were attacked by chloride ions and moisture present in the atmosphere. They were responsible for formation of corrosion pits which acted as initiation sites for stress corrosion cracks.
2. The residual stresses present in the material were responsible for crack propagation under the influence of electrochemical mechanism.
3. The $MgZn_2$ precipitation along the grain boundaries caused the anodic dissolution of grain boundaries resulting in intergranular SCC. The presence of chromium segregation and large network of sub-grain boundaries were also favorable for stress corrosion cracking.

Acknowledgment The authors are thankful to Director VSSC for his kind permission to publish this work. They further wish to thank Director LPSC Valiamala for referring the analysis and for supplying the specimens.

References

1. R.F. Muraca, J.S. Whittick, *Materials data handbook- Aluminium Alloy 7075*, 2nd edn. (Western applied research and development Inc, California, 1972)
2. S.D. Cramer, B.S. Bernard Jr., *Corrosion: Fundamentals, Testing and protection, ASM Handbook*, vol. 13A (ASM International, Materials Park, 2003)
3. E. John, *Hatch, Aluminum, Properties and Physical Metallurgy* (American Society for Metals, Ohio, 1984)
4. V.S. Raja, T. Shoji, *Stress Corrosion Cracking: Theory and Practise* (Woodhead Publishing Ltd, Cambridge, 2011)
5. M.O. Speidel, Stress Corrosion Cracking of Aluminum Alloys. *Metall. Trans. A* **6**, 631–651 (1975)
6. T.D. Burleigh, The postulated mechanisms for stress corrosion cracking of aluminum alloys- a review of the literature 1980–1989. *Corrosion* **49**, 89–98 (1991)
7. A.F. Oliveira Jr., M.C. De Barros, K.R. Cardoso, D.N. Travessa, The effect of RRA on the strength and SCC resistance on AA7050 and AA7150 aluminum alloys. *Mater. Sci. Eng. A* **379**(1–2), 321–326 (2004)
8. R. Ghosh, A. Venugopal, P. Sankarvelayudham, R. Panda, S.C. Sharma, K.M. George, V.S. Raja, Effect of thermomechanical treatment on the environmentally induced cracking behavior of AA7075 alloy. *J. Mater. Eng. Perform.* **24**(2), 545–555 (2015)
9. D.S. Mackenzie, G.E. Totten, *Analytical Characterization of Aluminium, Steel and Superalloys* (Taylor & Francis, London, 2006)